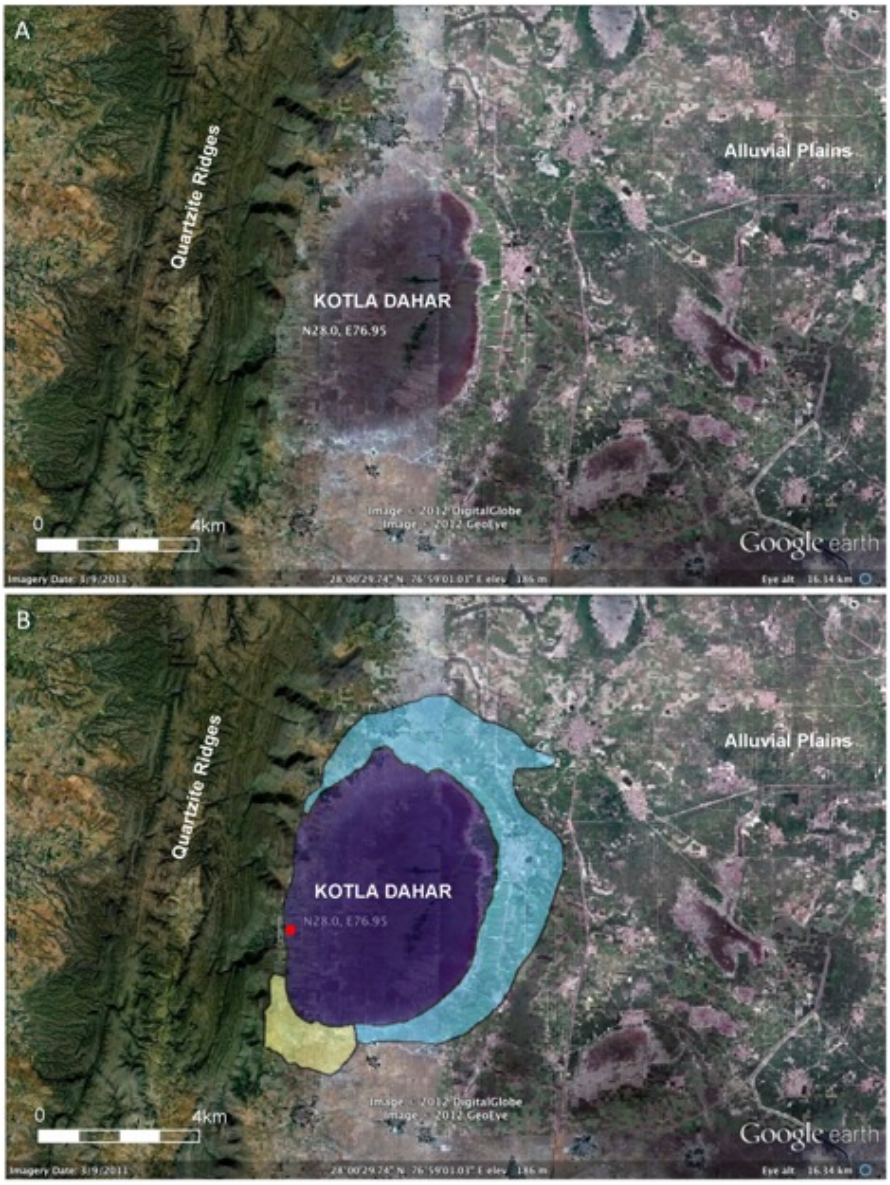

Figure DR1. (A) The Kotla Dahar basin lies east of Quartzite ridges in the alluvial plain of Mewat District of Haryana State, India (Saini et al., 2005). (B) Overlain on the photograph are the palustrine (light blue) and lacustrine (dark blue) areas and aeolian mounds (yellow) (after Saini et al., 2005). The sampled pit section (red star) is located at N28°00'095'', E76º57'173'' (Source: Google. (2013) Google Earth (Version 6.1) [Computer program]. Available at http://www.google.com/earth/download/ge/agree.html (Accessed 12 December 2012).

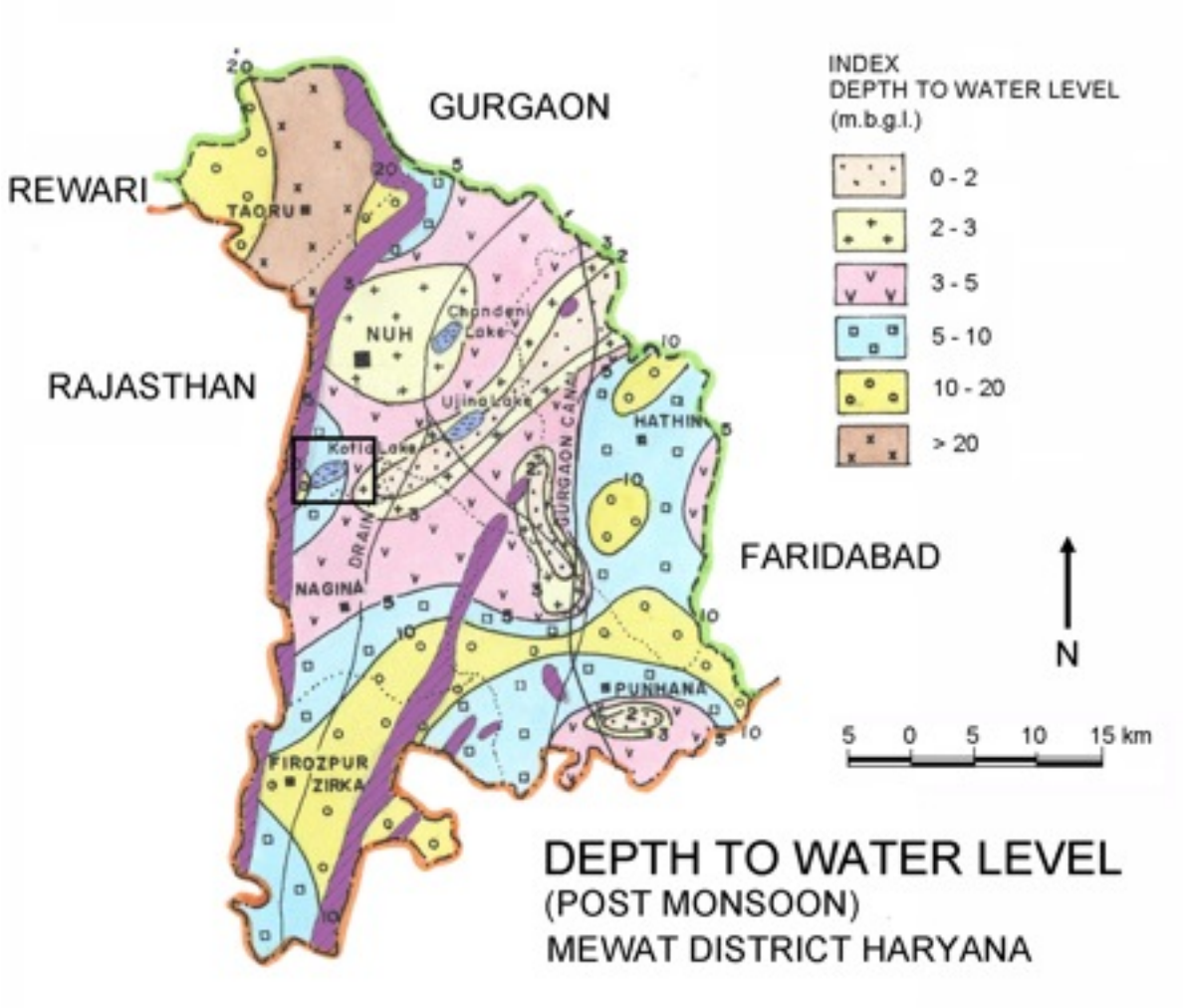

Figure DR2. Hydrogeology of Mewat district showing depth to water table during the monsoon period (Khan, 2007). Black box on this map designates the area shown in Fig. DR1.The NNE-SSW quartzite ridge (purple) to the west of Kotla Dahar acts as a ground water divide, as does the partial ridge (purple) to the southeast. Seasonal streams from the western ridge flow towards the southeast and fill natural depressions in the alluvial plain giving rise to lakes including modern Kotla Dahar, which is currently dry. During years of heavy rainfall extensive flooding occurs throughout the central area.

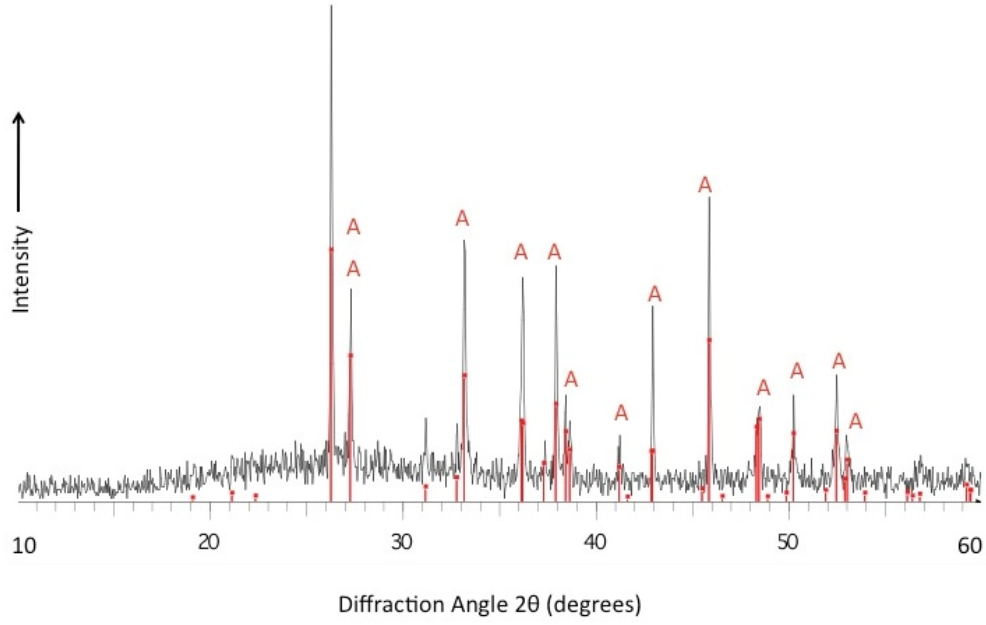

Figure DR3. Example of a well-preserved specimen of *Melanoides tuberculata*, representative of shells used for isotopes analysis and radiocarbon dating of Kotla Dahar section. *Melanoides tuberculata* is a prosobranch (gill- breathing) species that occurs abundantly in a wide range of fresh and brackish water habitats. *Melanoides tuberculata* was used for the oxygen-isotope analysis because it secretes its shell in near oxygen isotopic equilibrium with lake water (Shanahan et al., 2005). *M. tuberculata* is a littoral species that lives for 1 to 5 yrs and tolerates a wide range of fresh and brackish water habitats (Leng et al., 1999). X-ray powder diffraction (XRD) pattern of the shell with expected red peaks of pure aragonite.

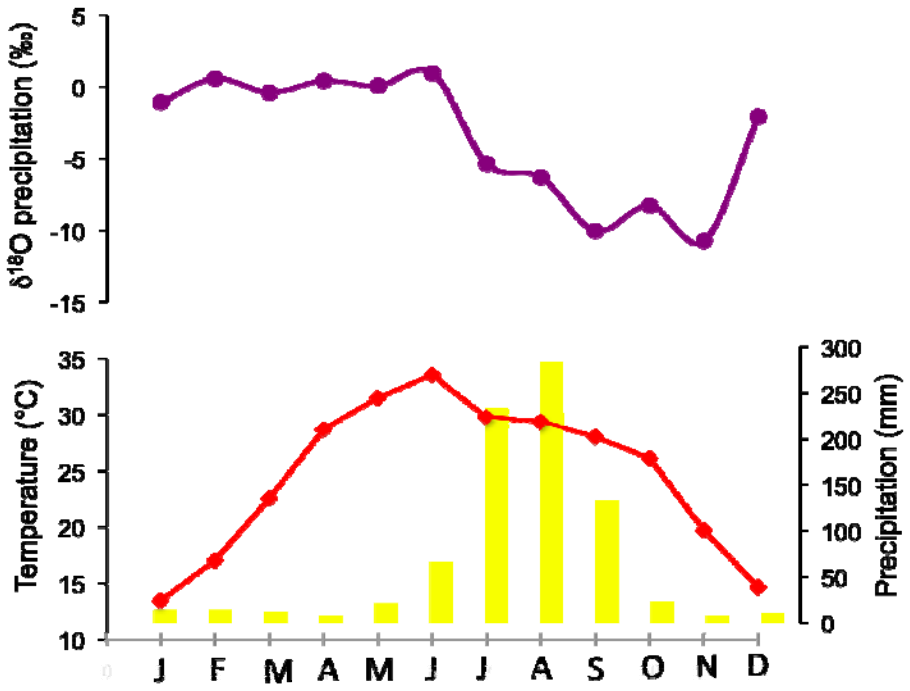

Figure DR4. Seasonal variations of $\delta^{18}O$ of precipitation (purple), monthly precipitation amount (yellow bars) and surface air temperature (red) from Global Network of Isotopes in Precipitation (GNIP) for New Delhi. Kotla Dahar lies 65 km SE of New Delhi, which is the nearest International Atomic Energy Association (IAEA) GNIP station where water isotope data are available. The low $\delta^{18}O$ values associated with maximum summer rainfall in July-Aug-Sept extend into October and November before increasing in December (Rozanski et al., 1993).

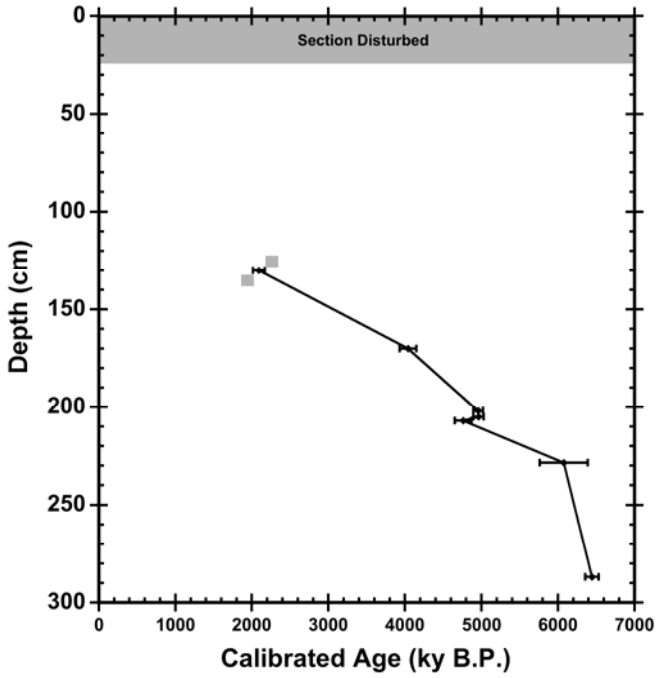

Figure DR5. Depth versus age plot for Kotla Dahar section. Radiocarbon dates were converted to calendar years using OxCal v.4.1.63 and the IntCal09 data set (Reimer et al., 2009). Calibrated age is reported over 2σ error range. Sediment depths were converted to age using equations derived by interpolation of depth-age points between the surface (assumed to be modern) to 130 cm, 130 to 170 cm, 170 to 202, 205, 207 cm and 207 to 228 cm. The mean age is used for the first two dated horizons at 125 and 135 cm (grey squares). Ages above the first dated sample at 130 cm were determined by interpolation between the surface (modern, equivalent to -43 radiocarbon yr) and 2,118±30 ^{14}C yr B.P. One radiocarbon date on shell fragments at 180-185 cm was excluded from the age model owing to poor preservation (Supplementary Figure DR6). Age estimation of the horizon of $\delta^{18}O_a$ increase at 175 cm*. The age range for 175 cm was calculated by best fit line between the dated horizons at 170 cm (3930-4040 yrs B.P.) and the ages obtained from 202, 205 and 207 cm (Fig. DR8).

Evaluation of Hard Water Lake Error Correction

Because it was not possible to find a horizon in the core where both shell and terrestrial organic carbon could be radiocarbon dated simultaneously, we evaluated hardwater lake error by extrapolating carbonate shells date to 228.5 cm where charcoal was dated.

Figure DR6 shows a regression line through all shell dates and the predicted age at 228.5 cm is younger than the charcoal date, which is opposite to that expected for hard-water lake error. Because the oldest radiocarbon date was on shell fragments, we removed this date and recalculated the regression line using six shell dates (Fig. DR7). Projection of the line to 228.5 cm gives the same age as the charcoal, supporting a negligible hard-water lake error for Kotla Dahar.

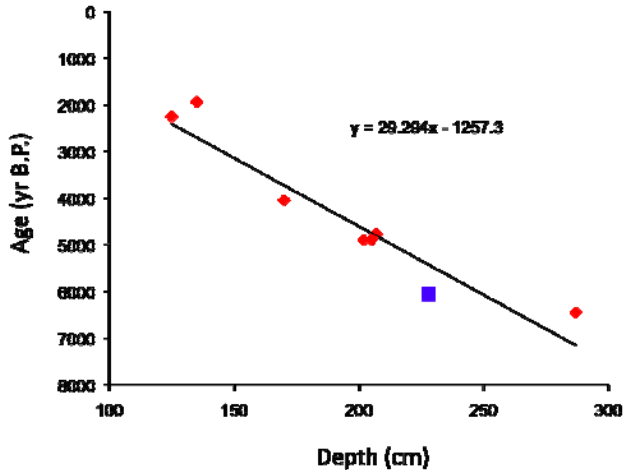

Figure DR6: Linear regression of calibrated radiocarbon dates on carbonates (red) and charcoal (blue). The charcoal date is older than the predicted carbonate age, which is the opposite expected from hard-water lake error.

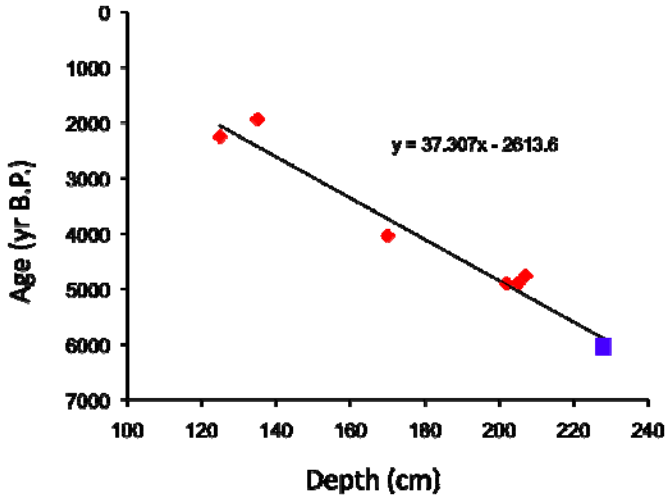

Figure DR7: Linear regression of calibrated radiocarbon dates on carbonates (red) and charcoal (blue). The charcoal date falls on the regression line indicating that the predicted carbonate date is same age as the charcoal, supporting a negligible hard water lake error.

Table DR1: Hard water lake error correction of 100- 300 ^{14}C yr B.P. of the estimated age of $\delta^{18}O_a$ transition at 175cm.

Depth	Age (^{14}C yr)	2σ error	HW error (^{14}C yr)	Corrected age (^{14}C yr)	Cal. age (yr B.P.)	2σ error	Age at 175 cm yr B.P.
170	3710	±35	100	3610	3951.5	117.5	
202	4300	±25	100	4200	4742.5	99.5	4060
205	4300	±35	100	4200	4733	113	
[illegible]	[illegible]	[illegible]	[illegible]	[illegible]	4699	12	
[illegible]	[illegible]	[illegible]	10	[illegible]	.5	7.	
[illegible]	4250	[illegible]	0	4150	[illegible]	5	

Depth	^{14}C age	2σ error	HW error (^{14}C yr)	Corrected age (^{14}C yr)	Cal. age (yr B.P.)	2σ error	Age at 175 cm yr B.P.
170	3710	±35	200	3510	3786.5	93.5	
202	4300	±25	200	4100	4665.5	142.5	3900
205	4300	±35	200	4100	4632	183	
207	4250	±35	200	4050	4605	183	

Depth	^{14}C age	2σ error	HW error (^{14}C yr)	Corrected age (^{14}C yr)	Cal. age (yr B.P.)	2σ error	Age at 175 cm yr B.P.
170	3710	±35	300	3410	3696	124	
202	4300	±25	300	4000	4471	51	3800
205	4300	±35	300	4000	4489.5	78.5	
207	4250	±35	300	3950	4404	115	

The calibrated age corrected for hard water lake error lies between 4060- 3800 yr B.P. The known archaeological dates for the Mature-urban to Late-urban transition (4.0-3.9 ky B.P.) have analytical uncertainties giving the calibrated error of more than 150 to 310 years (Shaffer, 1992; Staubwasser and Weiss, 2006). The estimated age of climate drying corrected for hard water error of 300 ^{14}C yr (4060-3800 ky B.P) is still within the calibrated archaeological age range.

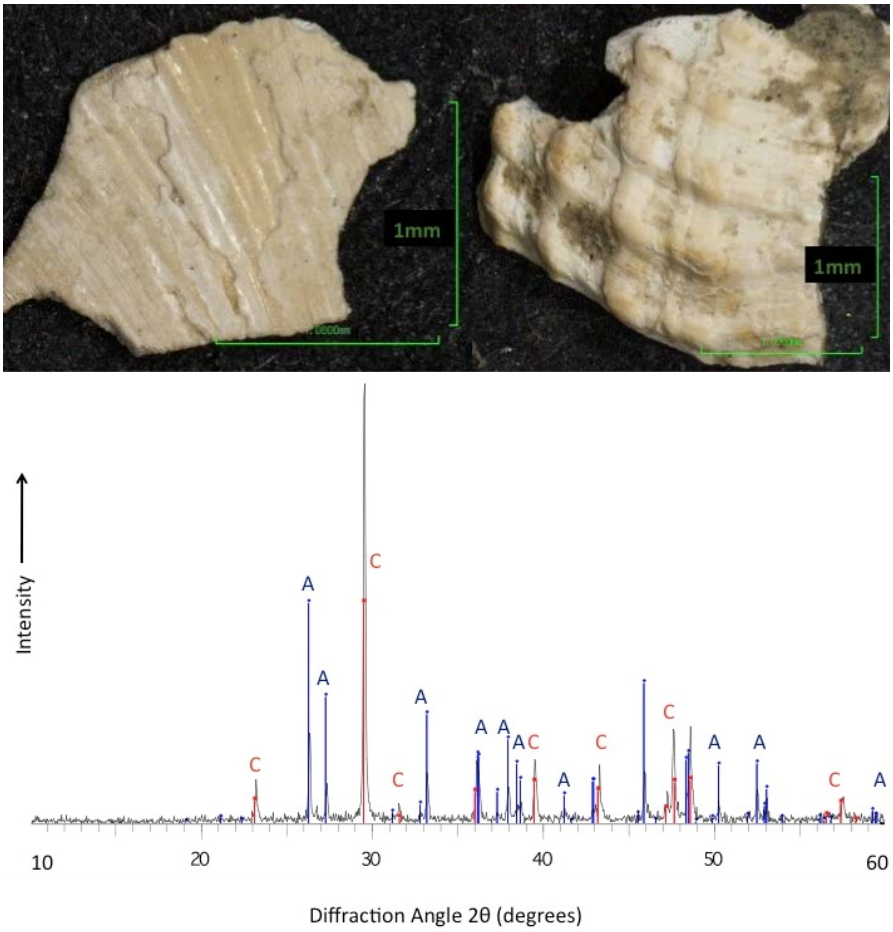

Figure DR8. Poorly preserved shell fragments from 180-185 cm showing evidence of diagenetic alteration. Further, XRD analysis indicates the shell fragments are composed of both calcite (red peaks) and aragonite (blue peaks) with calcite as the dominant mineral. This contrasts with whole shells of *M. tuberculata*, which are pure aragonite (Fig. DR2). We attempted to date these shell fragments at 180-185 cm but the radiocarbon age obtained from the shells was younger (3130±30 ^{14}C yr B.P.) than the horizon above at 170 cm (3710±30 ^{14}C yr B.P.). We reject this date on the basis of poor preservation.

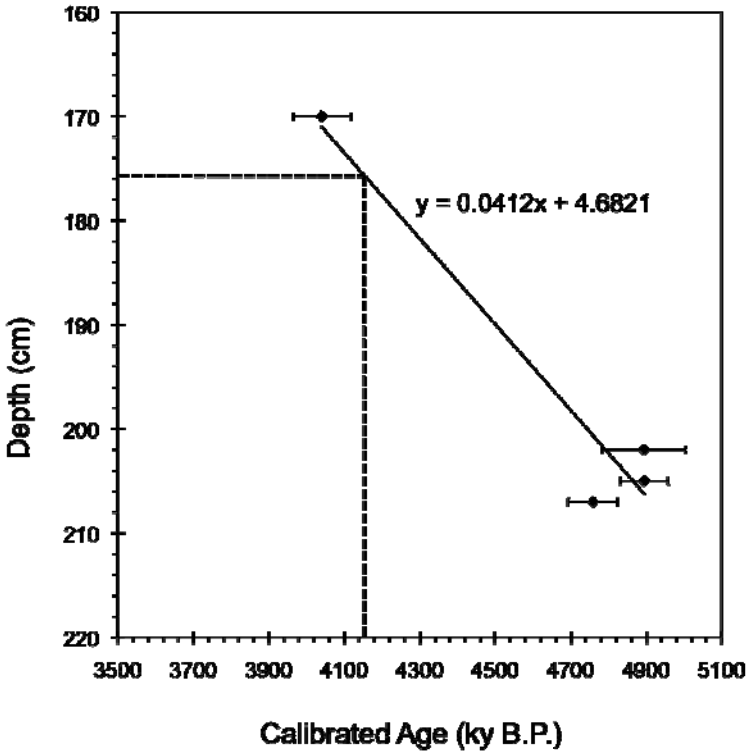

Figure DR9. Age and error estimate of the $\delta^{18}O_a$ increase at 175 cm. As the lithology of the section is the same below and above the transition in $\delta^{18}O_a$, the age of the transition at 175 cm was estimated by the best-fit line of the dates between 170, 202 cm, 205 and 207 cm.

Figure DR10. Various taxa of ostracods found in Kotla Dahar section. (A) *Ilyocypris*, (B) *Darwinula*, (C) *Faeformiscandona*, and (D) *Cyprideis torosa.* Presence of *Ilyocypris*, *Darwinula* and *Faeformiscandona* indicates fresh water conditions and *Cyprideis torosa* is indicative of more saline water.

Figure DR11: Photograph showing a pit being dug east of the quartzite ridges at paleolake bed in Kotla Dahar.

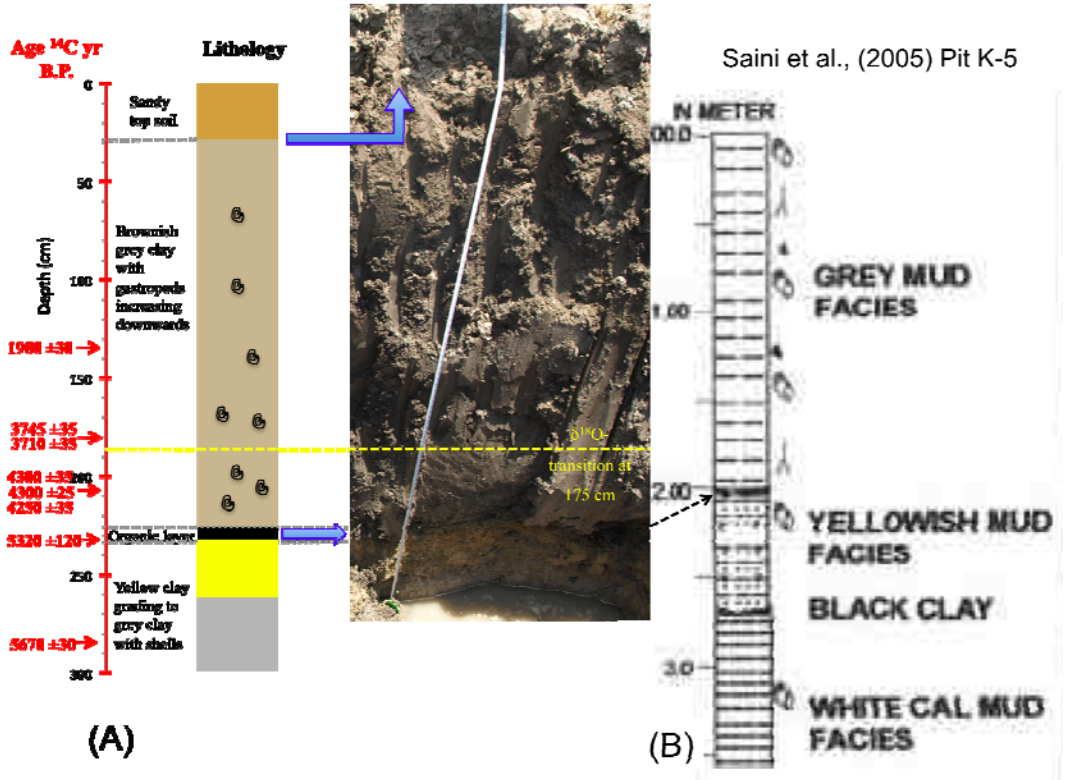

Figure DR12: Comparison of lithology of (A) Kotla Dahar section (this study) with, (B) (Saini et al., 2005) pit K-5. The radiocarbon dates (^{14}C yr) obtained from our section are shown in red. The lithology of the Kotla Dahar section consisted of four main units. The base of the section up to 2.31m is characterized by grey clay grading to yellow mud with abundant freshwater ostracods and the gastropod. This unit corresponds to white calcareous mud and yellowish mud facies in the pit K-5 described by (Saini et al., 2005). A ~5-cm thick black organic layer from 2.31-2.27 m caps the lower unit in our Kotla Dahar section. Saini et al.'s (2005) description of pit K-5 notes that there was a "yellowish mud facies that has 2–5 cm thick streaks of black clay", though the exact depth of the black clay is not reported. As seen in Figure DR12B, black clay is

shown between the top of the white mud facies and the bottom of the yellowish mud facies. However, there is also a black band shown between the top of the yellowish mud facies and the bottom of the grey mud facies, which is not identified in either image or text. No band of black clay is visible in the Kotla Dahar section reported here, and the relative position of the organic layer in our section corresponds to the position of the upper of the two black bands indicated in the pit K-5 section. The black organic layer is followed by brown-grey clay from 0.3-2.27m in our section corresponding to the grey mud facies 2m from to the top in Saini's pit K-5. The top 30cm in our section is yellow-brown sandy topsoil.

Methods and Materials

The top 30 cm of the 2.88-m section was discarded owing to the likelihood of human disturbance by cultivation. Consolidated deposits below 30 cm were sampled at 5-cm intervals to 2 m below the surface and at 1-cm intervals between 2 to 2.88 m. Samples for stable isotope analyses and ostracod fauna were wet sieved (at 63 microns) and dried overnight in an oven at 50°C prior to weighing. Ostracods were picked from ~25g of sediment sample and were counted using a binocular microscope at 10X magnification. Between 5-10 well-preserved specimens of the aragonitic gastropod *Melanoides tuberculata* (Supplementary Fig. DR2) were selected from each sample for isotope analysis. *M.tuberculata* shells were cracked open, sonicated in methanol and rinsed in double-distilled water to remove fine-grained clay particles. Oxygen isotope analysis was performed on homogenous powder of cleaned gastropod shell fragments at the University of Cambridge, with a VG SIRA Mass Spectrometer with Multicarb preparation system. Results are reported relative to the Vienna Pee Dee Belemnite (VPDB) standard. Analytical precision, based on analysis of the Carrara Marble standard, was ±0.1‰. Weight percent $CaCO_3$ of the sediments was measured using an AutoMateFX carbonate preparation system coupled to a UIC (Coulometrics) 5011 CO_2 coulometer. Analytical precision during the study was estimated by analysis of 94 reagent-grade $CaCO_3$ (100%) standards that yielded a mean and standard deviation (1σ) of 99.97±0.82%.

Radiocarbon analyses were performed on *M. tuberculata*, mixed gastropods and organic material. Typically between 5 and 10 gastropod specimens were gently crushed and cleaned with methanol and double distilled water. Prior to target preparation, shells were gently leached in dilute hydrochloric acid (1N) to remove the surface layer that is susceptible to diagenetic alteration.

References

Khan, S.A., 2007. Groundwater information booklet: Indian Ministry of Water Resources, Central Groundwater Board, Government of India: cgwb.gov.in/District_Profile/Haryana/Mewat.pdf

Leng, M., Lamb, A., Lamb, H., Telford, R., 1999, Paleoclimatic implications of isotopic data from modern and early Holocene shells of the freshwater snail Melanoides tuberculata, from lakes in the Ethiopian Rift Valley: Journal of Paleolimnology, v. 21, p. 97–106, doi:10.1023/A:1008079219280

Reimer, and 27 others, 2009, IntCal09 and Marine09 radiocarbon age calibration curves, 0-50,000 years cal BP: Radiocarbon, v. 51, p. 1111-1150.

Rozanski, K., Araguás-Araguás, L., Gonfiantini, R., 1993, Isotopic patterns in modern global precipitation: Geophysical Monograph Series, v.78, p. 1–36.

Saini, H.S., Tandon, S.K., Mujtaba, S.A.I., and Pant, N.C., 2005, Lake deposits of the northeastern margin of Thar Desert: Holocene (?) Palaeoclimatic implications: Current Science, v. 88, p. 1994-2000.

Shaffer, J.G., 1992, The Indus Valley, Baluchistan, and Helmand Traditions: Neolithic through Bronze Age, *in* Ehrich, R.W., ed., Chronologies in Old World Archaeology, Volumes 1&2, (Third edition): Chicago, University of Chicago Press, p. I.441–464, II.425–446.

Shanahan, T.M., Pigati, J.S., Dettman, D.L., Quade, J., 2005, Isotopic variability in the aragonite shells of freshwater gastropods living in springs with nearly constant temperature and isotopic composition. Geochimica et Cosmochimica Acta, v. 69, p. 3949–3966, doi:10.1016/j.gca.2005.03.049.

Staubwasser, M., and Weiss, H., 2006, Holocene climate and cultural evolution in late prehistoric,early historic West Asia: Quaternary Research, v. 66(3), p. 372-387.

Table DR2
$\delta^{18}O$

Depth(cm)	Age cal kyr BP	δ18O ‰ in *M. tuberculata*
30	0.5	2.09
35	0.6	-0.7
40	0.6	1.14
45	0.7	0.09
50	0.8	0.44
55	0.9	-1.05
60	1.0	3.68
65	1.0	3.15
70	1.1	-0.19
75	1.2	1.93
80	1.3	3.78
85	1.4	2.73
90	1.4	2.75
95	1.5	-0.26
100	1.6	1.75
105	1.7	1.73
110	1.8	3.75
115	1.9	0.63
120	1.9	6.58
125	2.0	0.64
130	2.1	1.71
135	2.3	5.31
140	2.6	1.05
155	3.3	6.05
160	3.6	3.18
170	4.0	4.35
175	4.1	-0.14
180	4.2	-2.57
190	4.4	-2.95
201	4.6	-1.39
203	4.7	-1.35
204	4.7	-0.97
205	4.7	-1.58
207	4.8	-0.65
209	4.9	-0.41
211	5.0	-0.68
213	5.1	-1.80
217	5.4	-0.46
219	5.5	0.59
221	5.6	-0.85
223	5.8	-0.95
224	5.8	0.34
225	5.9	-1.14
226	5.9	-1.32
226	5.9	0.61
227	6.0	0.64
228	6.1	0.34
229	6.1	-0.09
232	6.1	-1.78

233	6.1	-1.12
245	6.2	0.88
248	6.2	-2.51
249	6.2	-2.82
250	6.2	0.81
251	6.2	-0.44
252	6.2	1.25
254	6.2	-3.31
255	6.2	-0.63
257	6.3	-1.53
260	6.3	-2.80
261	6.3	-2.79
263	6.3	-3.62
265	6.3	-3.04
266	6.3	-1.83
267	6.3	-2.87
268	6.3	-4.84
269	6.3	-4.32
270	6.3	-2.22
271	6.3	-0.63
273	6.4	-3.35
274	6.4	-4.58
275	6.4	-1.12
276	6.4	-0.96
278	6.4	-2.52
279	6.4	-4.15
280	6.4	-1.57
281	6.4	-1.17
282	6.4	-4.92
284	6.4	-5.17
285	6.4	-3.25
286	6.4	-3.41
287	6.4	-3.38
288	6.5	-4.36

Ostracod Count

Depth (cm)	Age cal kyrBP	Ostracod count/25g
30	0.5	0
40	0.6	0
45	0.7	0
50	0.8	0
55	0.9	0
60	1.0	0
65	1.0	0
70	1.1	0
75	1.2	0
80	1.3	0
85	1.4	0
90	1.4	0
95	1.5	0
100	1.6	0
105	1.7	0
110	1.8	0
115	1.9	0
120	1.9	0
125	2.0	0
130	2.1	0
135	2.3	0
140	2.6	0
145	2.8	0
150	3.1	0
155	3.3	0
160	3.6	0
165	3.8	0
170	4.0	0
175	4.1	1
180	4.2	1
185	4.3	0
190	4.4	2
195	4.5	1
201	4.6	2
203	4.7	6
204	4.7	10
205	4.7	11
207	4.8	13
209	4.9	8
212	5.1	15
214	5.2	14
216	5.3	0
218	5.4	3
220	5.6	1
221	5.6	5
222	5.7	5
223	5.8	4
224	5.8	4
225	5.9	2
226	5.9	3

227	6.0	3
228	6.1	4
229	6.1	0
230	6.1	0
231	6.1	0
232	6.1	0
233	6.1	0
234	6.1	0
235	6.1	0
236	6.1	0
237	6.1	8
238	6.1	5
239	6.1	3
240	6.1	2
241	6.2	3
242	6.2	6
243	6.2	9
244	6.2	3
245	6.2	9
246	6.2	7
247	6.2	7
248	6.2	7
249	6.2	4
250	6.2	15
251	6.2	20
252	6.2	28
253	6.2	29
254	6.2	20
255	6.2	30
256	6.3	10
257	6.3	4
258	6.3	0
259	6.3	2
260	6.3	28
261	6.3	8
262	6.3	1
263	6.3	3
264	6.3	3
265	6.3	2
266	6.3	3
267	6.3	4
268	6.3	4
269	6.3	6
270	6.3	7
272	6.4	8
273	6.4	8
274	6.4	7
275	6.4	4
276	6.4	16
277	6.4	18
278	6.4	23
279	6.4	14

280	6.4	6
281	6.4	36
282	6.4	39
283	6.4	22
284	6.4	22
285	6.4	14
286	6.4	15
287	6.4	18

%$CaCO_3$

Depth (cm)	Age cal kyr B	%CaCO3
30	0.5	7.8
40	0.6	7.1
45	0.7	6.8
50	0.8	7.6
55	0.9	9.2
60	1.0	8.5
65	1.0	7.1
70	1.1	8.2
75	1.2	10.4
80	1.3	9.0
85	1.4	8.2
90	1.4	10.4
95	1.5	9.2
100	1.6	9.0
105	1.7	10.1
110	1.8	9.6
115	1.9	7.9
120	1.9	8.4
125	2.0	13.3
130	2.1	15.6
135	2.3	11.7
140	2.6	9.7
145	2.8	10.1
150	3.1	11.4
155	3.3	10.0
160	3.6	12.4
165	3.8	14.9
170	4.0	18.4
175	4.1	19.5
180	4.2	21.2
185	4.3	25.6
190	4.4	26.4
195	4.5	32.9
201	4.6	38.6
203	4.7	41.1
204	4.7	38.8
205	4.7	43.7
207	4.8	44.6
209	4.9	39.8
211	5.1	44.1
213	5.2	43.7
215	5.3	45.9
217	5.4	42.8
219	5.6	38.3
221	5.6	37.9
222	5.7	36.9
223	5.8	40.9
224	5.8	38.0
225	5.9	43.9
226	5.9	36.7

227	6.0	43.2
228	6.1	46.1
229	6.1	37.8
230	6.1	44.6
231	6.1	46.4
232	6.1	48.1
233	6.1	46.7
234	6.1	42.3
235	6.1	43.4
237	6.1	38.9
238	6.1	45.0
239	6.1	34.0
240	6.1	47.0
241	6.2	51.3
242	6.2	48.5
243	6.2	41.6
244	6.2	51.2
246	6.2	47.0
247	6.2	49.2
248	6.2	45.8
249	6.2	49.4
250	6.2	44.2
251	6.2	46.0
252	6.2	45.5
253	6.2	40.6
254	6.2	44.1
255	6.2	52.1
257	6.3	55.4
258	6.3	52.8
259	6.3	54.0
260	6.3	56.0
261	6.3	61.4
262	6.3	52.3
263	6.3	55.2
264	6.3	57.1
265	6.3	57.8
266	6.3	53.3
267	6.3	55.2
268	6.3	55.3
269	6.3	53.4
270	6.3	56.4
272	0.0	59.3
273	6.4	55.7
274	6.4	59.4
275	6.4	63.3
276	6.4	59.8
277	6.4	69.0
278	6.4	70.3
279	6.4	70.3
280	6.4	67.7
281	6.4	72.1
282	6.4	69.9

283	6.4	71.1
285	6.4	66.3
286	6.4	68.2
287	6.4	67.5
288	6.4	69.0